2020 IEEE International Conference on Systems, Man, and Cybernetics (SMC)
October 11-14, 2020. Toronto, Canada

Painting with the Eye: Understanding The Visual Field of the Human Eye with SSVEP

Danson Evan Garcia, Kai Wen Zheng, Yi Liu, Yi (Summer) Tao, Steve Mann
MannLab Canada, 330 Dundas Street West, Toronto, Ontario, M5T 1G5

***Abstract*—We present an investigation into the relationship between steady-state visually-evoked potentials (SSVEPs) and the magnitude, distance, shape, and spatial location of the flashing stimulus relative to the participant. We use a wearable electroencephalography (EEG) device with the addition of an external occipital electrode for the experiments. SSVEP responses are extracted using the lock-in amplifier and fast Fourier transform algorithms. We then map the responses to what the human eye sees. Our experiments pinpoint the optimal range of stimulus parameters required for stable SSVEP response, identify failure states for flashing stimulus, as well as create a visual map, a vidmap, of the participant's ability to see. The results show that locating the stimulus at the participant's central vision elicits stronger SSVEP response compared to the peripheral vision.**

***Index Terms*—Signal processing, visual field interactions, electroencephalogram (EEG), steady-state visually-evoked potentials (SSVEP).**

I. Background and Introduction

Vision is a critical ability that many rely on to maintain their quality of life [1]. Its loss or impairment can greatly impact an individual's ability to perform critical and basic tasks [2]. Despite its importance, the study of human vision and perception is a difficult process. Data collected in relation to human vision must either be gathered via testimony, activation taken from cellular responses, or neuroimaging techniques [3], [4]. The former may be imprecise and unreliable, while the latter two often requires expensive and dedicated equipment [5]–[7]. The emerging relevance of wearable technologies can help to bridge the gap between reliability and accessibility [8]–[10]. Understanding of human vision can not only give us a better grasp of our capabilities [11] but can also be applied to create healthcare applications that help people with visual disabilities (i.e. to monitor, or aid them in their visual tasks). Applications include wearable facial recognizers for prosopagnosia patients [12], wearable low vision glasses for people with blindness or partial vision to navigate [13], detect obstacles [14] and read text [15]. These applications can help those with visual disabilities reestablish social and cognitive functions.

If metaveillance is the sensing of sensing [16], [17], then metavision is the vision of vision. Through understanding and visualization of senses, human perceptual capabilities may be revealed [18], [19]. Wearable devices provide extensions to and are inextricably intertwined with our natural capabilities [20], [21]. We aim to show how wearable EEG devices can realize metavision and create a more holistic understanding of human perception.

As metavision and visual field reconstruction can be used to map out the responsive sections of the human eye, it may have applications in better understanding eye damage and vision loss. Blurry and inexact vision can be mapped out, as a form of visual testing, replacing the current testimonial based vision tests. This technique can be used to help people with visual disabilities for visual damage early detection, monitoring, and future restoration.

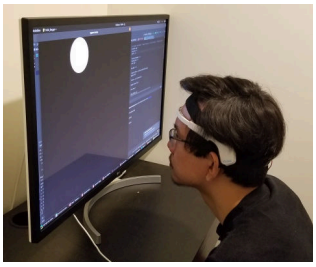

(a) An ayinography experiment.

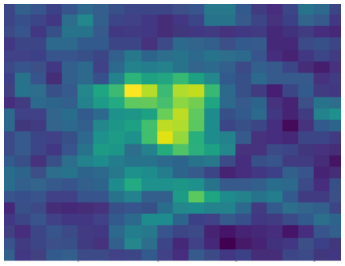

(b) Vidmap for 20 cm distance.

Fig. 1: a) is a photograph of the user taking the ayinography experiment. b) is a single slice of the participant's vidmap at 20 cm. The strength of the visual response peaks at the focal point, then slowly falling closer to the edges.

A. Steady-State Visually-Evoked Potentials (SSVEP)

A technique used widely in EEG research is the steady-state visually-evoked potential (SSVEP). SSVEP responses are natural periodic responses elicited by flickering visual stimuli at a specific frequency [6], [22]. Widely used in studies investigating spatial attention, these oscillatory responses are exhibited from frequencies of 1-90 Hz [23], [24] and are monitored using EEG or functional magnetic resonance imaging (fMRI) [6], [25]. However, steady and strong responses are only limited to a certain frequency range with the optimal frequency typically around 15 Hz [24].

B. Human Visual Perception

The inverse square law states that the intensity of the influence of a source is the source strength divided by the area of the sphere. Therefore the influence of a light source twice as far from the light source is spread over 4 times the area, hence $\frac{1}{4}$ the influence [26].

Objects can be seen by human eyes if they emit light themselves or reflect lights. Cells in the retina detect lights coming in the eyes. But vision is more complicated than just light hitting and being detected by light-receiving cells, the distance and spatial location of the stimulus relative to the fovea, and illuminance are important as well. Piper's law [27] states that the product of perceived intensity and the square root of the area is a constant, while Ricco's law [28] states that the product of area and perceived intensity is constant for the

threshold of excitation in the fovea of the human eye. These two different equations attempt to describe the eye's perception in different situations. A change of stimulus distance corresponds to an increase or decrease in stimulus size and illuminance. Prior studies have investigated the effect of stimulus distance on SSVEP response [29], [30].

C. Ayinography

Ayinography is a technique used to display the bioveillance flux of the human eye [18], [31]. Through a wearable EEG device, we capture and read the mind's interpretation of what we see, "mind's eye". Existing ayinographs uses an augmented reality overlay system to create the visual field in three-dimensional space. Such systems produce life-like representations of our mind's eye, with values based on changes in height and distance. However, creating a system from scratch may be difficult as the skills required are diverse. In this paper, we propose an ayinography that is purely done in software needing only a monitor to plot a two-dimensional representation of our mind's eye. Each representation, or "slice" of our visual field, can be taken across the width and height of our visual field, and also at different distances. The results may then be combined to create a full mapping of our visual field in three-dimensional space. Steve Mann proffers the resulting representation as a vidmap from the Latin words *videre* (which means to see) and *mappa* (which means a plane surface on which maps were drawn).

II. Methods

The EEG sensing device used during the experiments is the Muse Meditation Headband by InterAxon Inc. This wearable EEG device is shown in Fig. 2 with an extra electrode attachment. When worn, the external electrode is placed at the occipital lobe Oz position [32] to detect the SSVEP response.

Fig. 2: Left: Muse Headband with an external dry electrode. Right: Muse worn with a dry electrode at Oz position.

A. Algorithms

1) Fast Fourier Transform: Fast Fourier Transform [33] is an algorithm that computes the Discrete Fourier Transform (DFT) [34] from a sequence of points. It is an application of Fourier Analysis which converts a signal from its time domain to its corresponding frequency domain representation. The representation shows the power spectral components of the signal at various frequencies. In this paper, we apply FFT to detect the SSVEP response activations to various stimulus frequencies. A pronounced FFT peak at the target stimulus frequencies is indicative of a strong SSVEP response.

2) Lock-in Amplifier: A lock-in amplifier (LIA) is a device that can find and boost a reference signal frequency while eliminating other frequencies [35], [36]. An LIA device can determine a signal from its noisy environment so long as the reference signal is known. Modern LIAs typically implement a second reference signal, which is $90°$ phase-shifted from the original signal. This is to ensure the phase-independence of the source signal and the reference signal. For our implementation of a software-defined LIA, the raw EEG data is multiplied by a reference wave at the target frequency. The same raw EEG data is also multiplied by the $90°$ phase-shifted reference wave. These two results are then passed through a Butterworth low-pass filter to retrieve their LIA outputs. The magnitude of the two low-passed outputs is obtained and averaged over the specified time window.

B. Experimental Procedure

A particular stimulus frequency is selected based on the SSVEP response data from the participant. To determine the frequency in which the participant has a faster response while having a steady activation throughout, a task where a flickering stimulus window of a white and a black image. The flickering rate is set at frequencies from $5\,\text{Hz}$ to $20\,\text{Hz}$ at $0.5\,\text{Hz}$ increments, because evidence from previous studies confirm that steady and strong SSVEP response is typically around 15 hz [24]. At each increment, the stimulus flashes for $10\,\text{s}$ with a $3\,\text{s}$ rest in between frequencies, this is to ensure the response and desponse time for SSVEP response signals is captured in the data. From our previous experiment, we found that this response and desponse time varies from $1\,\text{s}$ to $2\,\text{s}$, thus a $10\,\text{s}$ flash interval will allow us to see whether or not the SSVEP response is steady, while the $3\,\text{s}$ resting period will show the full desponse duration for the frequency in question.

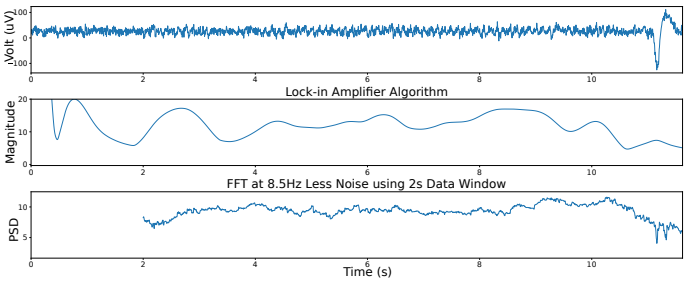

Fig. 3: $8.5\,\text{Hz}$ frequency test graph from a user. The top is the raw EEG data. The middle is the magnitude output using the lock-in amplifier algorithm. The bottom is the FFT power spectral density (PSD) at $8.5\,\text{Hz}$ less noise using a 2-second data capture window (i.e. 512 samples at $256\,\text{Hz}$ sampling frequency).

An example of an optimal SSVEP response is shown in Fig. 3. From both the lock-in amplifier and FFT graphs, A steady activation persists from 2 to $10\,\text{s}$. This is followed by a linear decrease in response that coincides with the stimulus ending at the $10\,\text{s}$ mark. The linear decrease after $10\,\text{s}$ represents the response delay time. Activation graphs that are not optimal

for the experiments typically show slower and more unstable activation and deactivation.

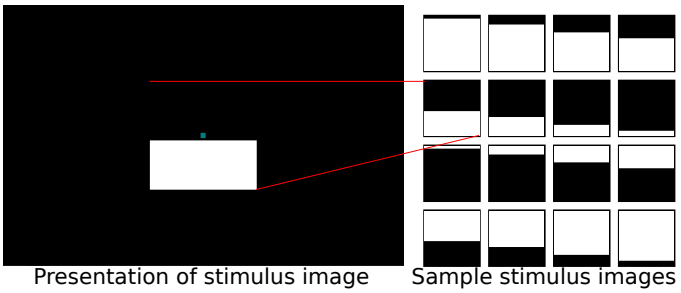

Fig. 4: A sample set of 400×400 px stimulus images and the corresponding presentation as a stimulus. The stimulus is flickered by changing between a full black image and the stimulus image.

After a stimulus frequency is selected, a set of experiment images are generated to test subjects' visual field coverage and his SSVEP response to different types of visual stimuli. These images are then presented on a black screen as shown in Fig. 4. Each stimulus image is 400×400 px, preferably about $\frac{1}{9}$ to $\frac{1}{12}$ of the total screen size. This size ensures that the image is large enough to elicit SSVEP responses but small enough to be within the user's visual field. Changing the image resolution is possible, especially if the screen resolution drastically changes the image display size.

To induce flickering at a particular stimulus frequency, a black foreground alternates with the stimulus image. A bluish-green indicator is also present on the screen. The 3-pixel tall indicator guides the user's visual focus. Subjects are asked to focus on and follow the indicator if it changes locations on the screen.

As the attention of the user is focused on the indicator and the stimulus, the user's EEG data are collected and timestamped. Each of the windowed stimulus images is also timestamped as they appear on the screen. These ensure that the EEG data can be mapped to a particular stimulus. The gathered EEG data from the Oz position are then processed using either the FFT method or the LIA method depending on the experiment's needs.

III. Results and Discussion

A. Observations with Non-uniform Patterns

We examine how different stimulus patterns affect the resulting SSVEP response at the stimulus frequency. In the experiment, subjects are tested with four sets of stimulus patterns as shown in Fig. 5. Fig. 5a and 5b were selected to gain insight into the peripheral vision and the effects of black and white pixels ratios on SSVEP. Additionally, we chose Fig. 5c and 5d with expanding black and white circles to measure the significance of the visual center in producing SSVEP response. The ratio of black and white in each set of the stimulus images changes in each frames. The stimulus images are presented individually at the center of the screen with a stationary center indicator. During the experiment, the subject focuses their vision at the center of each stimulus image. The stimulus image flickers for 10 s followed by a 3 s rest before it changes into another image with increasing frame count.

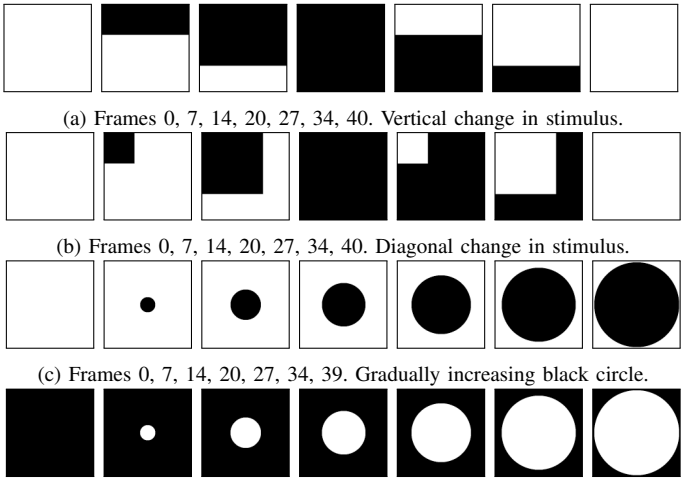

(a) Frames 0, 7, 14, 20, 27, 34, 40. Vertical change in stimulus.

(b) Frames 0, 7, 14, 20, 27, 34, 40. Diagonal change in stimulus.

(c) Frames 0, 7, 14, 20, 27, 34, 39. Gradually increasing black circle.

(d) Frames 0, 7, 14, 20, 27, 34, 39. Gradually increasing white circle.

Fig. 5: Sets of stimuli used with non-uniform patterns. a) and b) are stimuli that change from fully white to fully black then to fully white. c) and d) are stimuli that have a circle with increasing size in the middle.

In each set of stimulus patterns, we consider two factors that affect the level of SSVEP activation which is shown in Fig. 6. First is the ratio of the white pixels in the 400×400 px stimulus window. This is directly related to the amount of stimulus flicker the subject is exposed to since the stimulus image alternates with a black image window. This ratio is represented by the y-axis on the graphs. The second factor is whether the white portion of the stimulus window overlaps with the participant's visual focus. This allows us to understand the extent of a person's visual acuity by seeing the effects of peripheral and focused stimuli to SSVEP activation. The green dots represent frames of images with white pixels that overlap with participants' visual focus and red dots otherwise.

The set of stimuli in Fig. 6a and 6b both have ratios of white pixels that decreases to 0 and increases back to 1. The variations in Fig. 6a has a constant rate while Fig. 6b has an exponential rate attributed to two-dimensional nature of images. The set of stimuli in Fig. 6c and 6d are inverse of each other. Their variations are exponentially decreasing and increasing, respectively.

The FFT PSD results from the experiment are shown in Fig. 7. The two-dimensional heatmap represents the changing FFT PSD for each set of stimuli with respect to the stimulus frame number. The PSD results are in log-scale less than the average noise floor obtained for a 10-second data capture window.

From the graphs, correlations between the stimulus frequency and SSVEP response frequency is clear. The peak SSVEP activation is constantly at 8.5 Hz. The activation intensity is also noticeably related to the ratio of the white pixels present and its overlap with the visual focus of the subject.

For both Fig. 7a and 7b, peak activation happens from frame 0 to 10 and from frame 30 to 40. Fig. 6a and 6b shows that those frames correspond to frames where white pixels overlap with

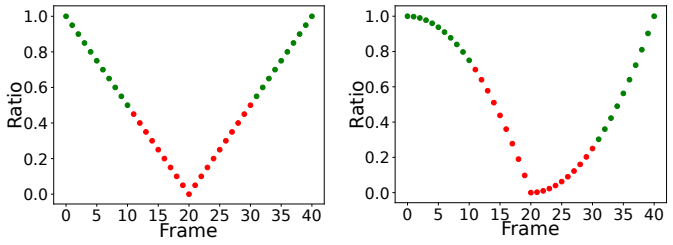

(a) Graph for stimulus set in Fig. 5a. (b) Graph for stimulus set in Fig. 5b.

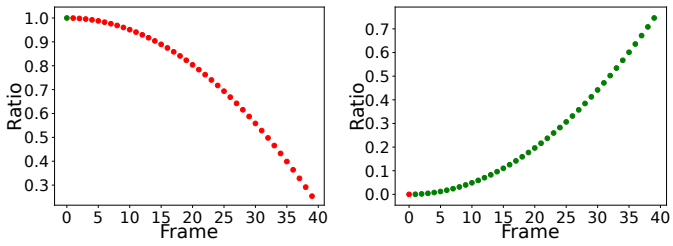

(c) Graph for stimulus set in Fig. 5c. (d) Graph for stimulus set in Fig. 5d.

Fig. 6: Percentage of white pixels in the stimulus window. The green points represent when the middle point of the window contains a white pixel while the red points show its absence. The x-axis is the frame number from the set of stimuli in Fig. 5.

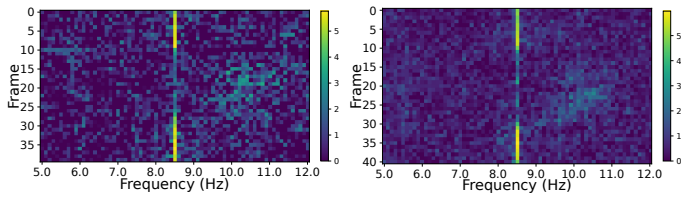

(a) FFT PSD heat map for Fig. 6a. (b) FFT PSD heat map for Fig. 6b.

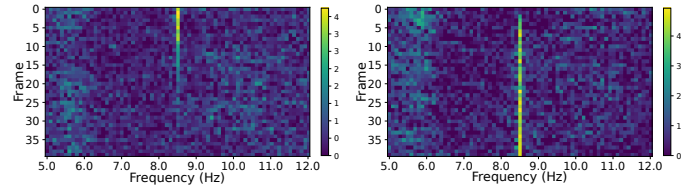

(c) FFT PSD heat map for Fig. 6c. (d) FFT PSD heat map for Fig. 6d.

Fig. 7: Heat maps showing the FFT PSD in log-scale less than the average noise floor from 5 to 20 Hz for each set of stimuli in Fig. 5. Each stimuli is flickered at 8.5 Hz for 10 s with a 3 s rest in between. The FFT is taken using a 10-second data capture window.

the subject's visual focus. Additionally, the absence of stable peak activation is visibly seen for the other frames. Based on this, the sudden absence and presence of stable peak activation indicates a non-linear relationship between the ratio of white pixels to the SSVEP response. In other words, the effects from the focal point overlap dominates the effects from the ratio of the white pixels.

We further show the non-linear relationship with Fig. 7c and 7d, which show decreasing and increasing peak activation respectively. In these sets of patterns, there is a dramatic change in color at the center pixel. In Fig. 6c, the center pixel changes immediately from white to black after the first frame and vice versa in Fig. 6d. In Fig. 7c, the largest drop in peak activation happens at the 9th frame, where the ratio of the white pixels is

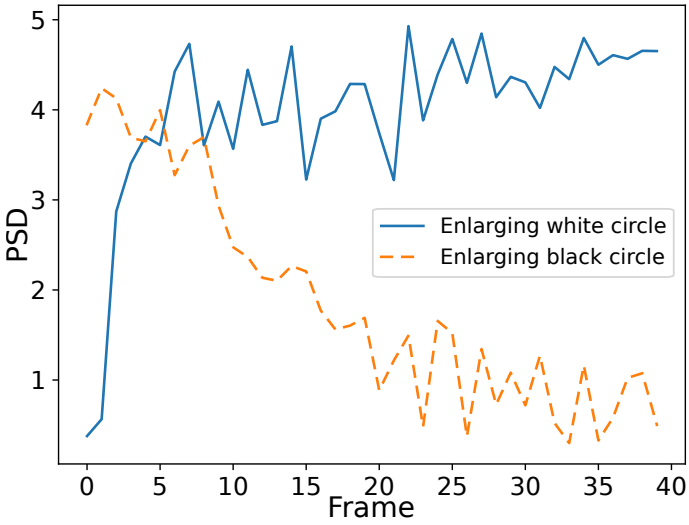

Fig. 8: Activation amplitudes at 8.5 Hz for stimuli shown in Fig. 5c and 5d. Orange line shows activation for Fig. 5c and blue line show activation for Fig. 5d.

0.969. In Fig. 7d, activation is present from the 3rd frame with a merely 0.002 white pixel ratio and continues to increase until it reaches a peak at around the 8th frame, with the corresponding white pixel ratio 0.024. Fig. 8 shows amplitude changes for these two stimuli over frames. None of the two curves shown are similar to ratio curves shown in Fig. 6a and 6b. Significant increase and decrease happen very soon after the appearance and disappearance of focal point pixel. Again, this indicates the effects from the focal point dominate the effects from the ratio of the white pixels.

B. Investigations with Ayinography

An ayinography is used to represent the degree to which human eyes can see at specific points in space. In this experiment, subjects place their visual focus at a stationary 3-pixel tall indicator at the center of the screen. A flashing white circle acts as the stimulus and this stimulus moves left to right and top to bottom. At each stimulus location, the stimulus flashes for a certain duration before moving to the next location at a fixed step size. Once the EEG data are collected, the data are processed using the LIA method. The corresponding output is a 23×23 px vidmap of the participant's field of vision as determined by the SSVEP response. To understand how distance affects the visual field, the subjects repeat the experiments at varying distances of their eye from the screen. The resolution of the human eye (the receptive field size) is approximately one arc-minute in the center (the fovea) but the size increases in peripheral vision [37]. Therefore, the fovea has a higher resolution and should lead to a higher SSVEP response to stimuli.

Fig. 9 shows the vidmaps of User A's visual field starting at 20 cm, and at 10 cm intervals afterwards, ending at 60 cm. These vidmaps are then stitched together to form a three-dimensional representation of the visual field, a 3-D ayinograph. As indicated by the two red lines, the activation in the vidmap is more condensed at 20 cm and more spread out as distance increased. However, as indicated by the white lines,

as distance increases, the intensity decreases as the activation gets more spread out, but we always have the highest activation at the focal point and the activation at the peripheral drops as distance increases from the focal point.

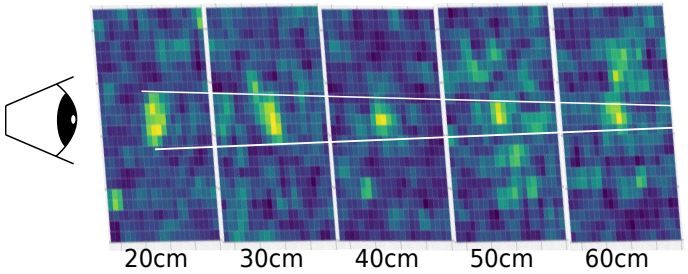

Fig. 9: Vidmaps at different distances from a screen using SSVEP response at 8.5 Hz from User A. A 200 × 200 px circle stimulus traverses, left to right, top to bottom, while the subject's visual focus is at the center of the screen. The stimulus flashes for 1 s at each location and moves by 40 px step sizes.

To understand this phenomenon better, a second ayinograph from another participant, User B was taken. Fig. 10 shows the vidmaps at similar 10 cm intervals. Aside from having different users, another difference between the two ayinographs is that the stimulus flashes for 2 s at each location in Fig. 10 instead of the 1 s in Fig. 9. The additional stimulus exposure time visibly increases the intensity at the focal point and also the activation spreads much faster.

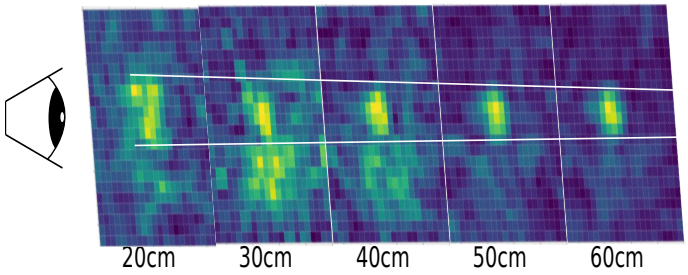

Fig. 10: Vidmaps at different distances from a screen using SSVEP response at 8.5 Hz from User B. A 200 × 200 px circle stimulus traverses, left to right, top to bottom, while the subject's visual focus is at the center of the screen. The stimulus flashes for 2 s at each location and moves by 40 px step sizes.

The results from both ayinographs show that as distance increases, the area of high activation at the center decreases slightly. The increased distance also makes the SSVEP response to spread out more from the center as the participant's visual field becomes larger.

C. Sketches with the Human Eye

In this experiment, the original image is presented on the screen flashing at the stimulus frequency with a moving 3-pixel tall indicator, which cues the subject's visual focus. The stimulus window slides across the screen left to right and top to bottom. The stimulus window flashes for a fixed duration at each location and moves to a new location with a fixed step size. This way of stimulus presentation is analogous to the natural eye movement pattern when reading.

Fig. 11 illustrates this experiment. From Fig. 11a, the entire star image is flickered at 8.5 Hz. The subject focuses on

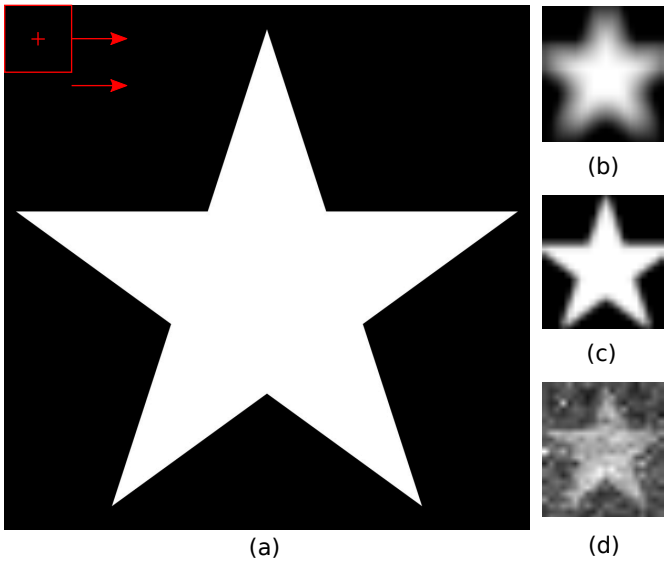

Fig. 11: a) The entire star image is flickered at 8.5 Hz while a stimulus window, illustrated in red, is moving left to right and top to bottom. The window is hidden and the participant only sees a 3-pixel tall indicator at the window center where they have to focus. The 200 × 200 px window moves every 2 s by 40 px step sizes. b) and c) are the target average bitmap and Gaussian bitmap of a) respectively. d) is the lock-in amplifier reconstruction of a).

the center (marked as a red cross) of an imaginary stimulus window, shown in red. The 200 × 200 px stimulus window stays at a location for 2 s and then moves across the screen as indicated by the arrows with a 40 px step size. Fig. 11b is the resulting bitmap that takes the ratio of the white pixel in a stimulus window and maps this ratio into a single pixel. We refer to this as the target average bitmap. Fig. 11c is the resulting bitmap that takes puts a higher weight on the center of the window, resulting in each pixel being a Gaussian representation of a stimulus window. We refer to this as the target Gaussian bitmap. Once the EEG data is collected for the experiment, the data is processed using the LIA method. The resulting bitmap for the star is shown in Fig. 11d.

From the reconstruction of the star image, we can visibly reason that our "mind's" eyes follow the Gaussian bitmap representation more closely than the average bitmap representation. All the edges of the star are sharp and the image is crisp.

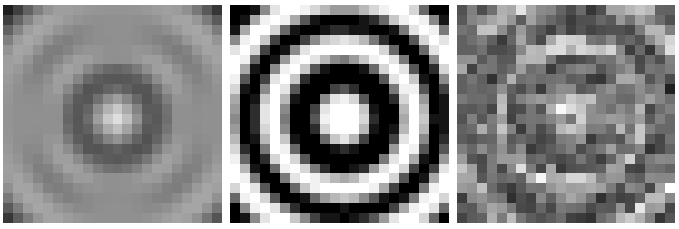

Fig. 12: A bullseye target image to illustrate further that our eye puts a larger weight at the center of focus instead of average around a window. The entire image is flickered at 8.5 Hz with a 200 × 200 px window, moving every 2 s by 40 px step sizes. a) and b) are the target average bitmap and Gaussian bitmap of a) respectively. c) is the lock-in amplifier reconstruction.

To further investigate this visual property, we examine a

much harder moving stimulus window reconstruction of a bullseye target in Fig. 12. Fig. 12a clearly shows that the target average bitmap is blurry to the point that it is hard to distinguish the distinct black and white concentric areas. On the other hand, Fig. 12b still shows distinguishable concentric blacks and whites. The reconstruction in Fig. 12c is more similar to the Gaussian bitmap. The averaged bitmap shows that the rings of the target should be heavily blurred in the naive case, where SSVEP response is equally distributed to all parts of the eye. However, in reality, the resultant data shows clearly defined rings and center dot. This resultant image much more closely matches with the Gaussian bitmapping.

IV. Conclusion

In this paper, we investigated the relationship of SSVEP response and the visual field of the human eye. We used FFT and LIA algorithms to extract these responses and designed experiments to study the effects of stimulus distance, shape, and spatial location. In doing so, we discovered that the presence of stimulus at the central vision greatly influences the SSVEP response.

V. Acknowledgements

Thanks to InteraXon Inc. for donating the Muse headsets. We also received funding from Ford Motor Company and the University of Toronto Faculty of Information, which will help us continue this work going forward at the University of Toronto.

References

[1] G. C. Brown, "Vision and quality-of-life." *Transactions of the American Ophthalmological Society*, vol. 97, p. 473, 1999.

[2] J. S. Rahi, P. M. Cumberland, and C. S. Peckham, "Visual impairment and vision-related quality of life in working-age adults: findings in the 1958 british birth cohort," *Ophthalmology*, vol. 116, no. 2, pp. 270–274, 2009.

[3] S. Sue, "Test distance vision using a Snellen chart." *Community Eye Health*, vol. 20, no. 63, p. 52, 2007.

[4] D. Cao, N. Nicandro, and P. A. Barrionuevo, "A five-primary photostimulator suitable for studying intrinsically photosensitive retinal ganglion cell functions in humans," *Journal of vision*, vol. 15, no. 1, pp. 27–27, 2015.

[5] J. E. Lovie-Kitchin, "Validity and reliability of visual acuity measurements," *Ophthalmic and physiological optics*, vol. 8, no. 4, pp. 363–370, 1988.

[6] A. M. Norcia, L. G. Appelbaum *et al.*, "The steady-state visual evoked potential in vision research: a review," *Journal of vision*, vol. 15, no. 6, pp. 4–4, 2015.

[7] V. Mihajlović, B. Grundlehner *et al.*, "Wearable, wireless EEG solutions in daily life applications: what are we missing?" *IEEE journal of biomedical and health informatics*, vol. 19, no. 1, pp. 6–21, 2014.

[8] S. Mann, "Wearable computing: A first step toward personal imaging," *Computer*, vol. 30, no. 2, pp. 25–32, 1997.

[9] S. Mann *et al.*, "Wearable, tetherless computer–mediated reality: WearCam as a wearable face–recognizer, and other applications for the disabled," in *Presentation at the American Association of Artificial Intelligence, 1996 Symposium. Retrieved January*, vol. 21, 1996, p. 2002.

[10] S. Mann, "Wearable computing as means for personal empowerment," in *Proc. 3rd Int. Conf. on Wearable Computing (ICWC)*, 1998, pp. 51–59.

[11] D. E. Garcia, K. W. Zheng *et al.*, "Capturing pictures from human vision using SSVEP and lock-in amplifier," in *33rd Conference on Graphics, Patterns and Images*. Porto de Galinhas, Brazil: IEEE, In Press, 2020.

[12] K. Y. R. Lu and S. Yanushkevich, "Wearable system-on-module for prosopagnosia rehabilitation," in *2016 IEEE Canadian Conference on Electrical and Computer Engineering (CCECE)*. IEEE, 2016, pp. 1–4.

[13] T. H. Riehle, P. Lichter, and N. A. Giudice, "An indoor navigation system to support the visually impaired," in *2008 30th Annual International Conference of the IEEE Engineering in Medicine and Biology Society*. IEEE, 2008, pp. 4435–4438.

[14] R. K. Katzschmann, B. Araki, and D. Rus, "Safe local navigation for visually impaired users with a time-of-flight and haptic feedback device," *IEEE Transactions on Neural Systems and Rehabilitation Engineering*, vol. 26, no. 3, pp. 583–593, 2018.

[15] R. Shilkrot, J. Huber *et al.*, "FingerReader: a wearable device to support text reading on the go," in *CHI'14 Extended Abstracts on Human Factors in Computing Systems*, 2014, pp. 2359–2364.

[16] S. Mann, "Surveillance (oversight), sousveillance (undersight), and metaveillance (seeing sight itself)," *2016 IEEE Conference on Computer Vision and Pattern Recognition Workshops (CVPRW)*, 2016.

[17] ——, "Phenomenological augmented reality with the sequential wave imprinting machine (SWIM)," in *2018 IEEE Games, Entertainment, Media Conference (GEM)*. IEEE, 2018, pp. 1–9.

[18] S. Mann, S. Feiner *et al.*, "Wearable computing, 3D aug* reality, photographic/videographic gesture sensing, and veillance," in *Proceedings of the Ninth International Conference on Tangible, Embedded, and Embodied Interaction*, 2015, pp. 497–500.

[19] R. Janzen and S. Mann, "Sensory flux from the eye: Biological sensing-of-sensing (veillametrics) for 3D augmented-reality environments," *2015 IEEE Games Entertainment Media Conference (GEM)*, 2015.

[20] S. Mann, *Humanistic Intelligence as a Basis for Intelligent Image Processing*. Wiley-IEEE Press, 2002.

[21] ——, "Humanistic intelligence," *Proc. Ars Electronica*, pp. 8–13, 1997.

[22] R. C. Panicker, S. Puthusserypady, and Y. Sun, "An asynchronous P300 BCI with SSVEP-based control state detection," *IEEE Transactions on Biomedical Engineering*, vol. 58, no. 6, p. 1781–1788, 2011.

[23] C. S. Herrmann, "Human EEG responses to 1-100 Hz flicker: resonance phenomena in visual cortex and their potential correlation to cognitive phenomena," *Experimental Brain Research*, vol. 137, no. 3-4, p. 346–353, Feb 2001.

[24] M. A. Pastor, J. Artieda *et al.*, "Human cerebral activation during steady-state visual-evoked responses," *The Journal of Neuroscience*, vol. 23, no. 37, p. 11621–11627, 2003.

[25] S. A. Hillyard, H. Hinrichs *et al.*, "Combining steady-state visual evoked potentials and fMRI to localize brain activity during selective attention," *Human Brain Mapping*, vol. 5, no. 4, p. 287–292, 1997.

[26] F. Vera, R. Rivera, and M. Ortíz, "A simple experiment to measure the inverse square law of light in daylight conditions," *European Journal of Physics*, vol. 35, no. 1, p. 015015, 2013.

[27] H. Piper, "Uber die abhangigkeit des reizwertes leuchtender objekte von ihrer flachen-bezsw. winkelgrosse," *Zeitschrift fur Psychologie und Physiologie der Sinnesorgane*, vol. 32, pp. 98–112, 1903.

[28] A. Riccò, "Relazione fra il minimo angolo visuale e l'intensità luminosa." *Memorie della Societa Degli Spettroscopisti Italiani*, vol. 6, pp. B29–B58, 1877.

[29] C.-H. Wu and H. Lakany, "The effect of the viewing distance of stimulus on SSVEP response for use in brain-computer interfaces," in *2013 IEEE International Conference on Systems, Man, and Cybernetics*. IEEE, 2013, pp. 1840–1845.

[30] N. Kwak, D. Won *et al.*, "Analysis of steady state visual evoked potentials based on viewing distance changes for brain-machine interface speller," in *2016 IEEE International Conference on Systems, Man, and Cybernetics (SMC)*, 2016, pp. 001 502–001 505.

[31] S. Mann, D. Defaz *et al.*, "Encephalogames (brain/mind games): Inclusive health and wellbeing for people of all abilities," in *2019 IEEE Games, Entertainment, Media Conference (GEM)*. IEEE, 2019, pp. 1–10.

[32] H. Jasper, "Report of the committee on methods of clinical examination in electroencephalography," *Electroencephalogr Clin Neurophysiol*, vol. 10, pp. 370–375, 1958.

[33] C. Van Loan, *Computational frameworks for the fast Fourier transform*. Siam, 1992, vol. 10.

[34] T. M. Peters and J. H. T. Bates, "The discrete Fourier transform and the fast Fourier transform," *The Fourier Transform in Biomedical Engineering*, p. 175–194, 1998.

[35] S. Devore, A. Gauthier *et al.*, "Improving students understanding of lock-in amplifiers," *2013 Physics Education Research Conference Proceedings*, Jan 2014.

[36] J. H. Scofield, "Frequency-domain description of a lock-in amplifier," *American journal of physics*, vol. 62, no. 2, pp. 129–133, 1994.

[37] M. Glickstein, *Neuroscience: A historical introduction*. MIT Press, 2014.